INTERNATIONAL JOURNAL OF HYDROGEN ENERGY 40 (2015) 15865–15876

Available online at www.sciencedirect.com

ScienceDirect

journal homepage: www.elsevier.com/locate/he

Hydrogen production by steam reforming of DME in a large scale CFB reactor. Part I: Computational model and predictions

Francis A. Elewuwa [a], *Yassir T. Makkawi* [b,*]

[a] *European Bioenergy Research Institute (EBRI), School of Engineering and Applied Science, Aston University, Birmingham B4 7ET, UK*

[b] *Chemical Engineering Department, American University of Sharjah, P.O. Box 26666, Sharjah, United Arab Emirates*

ARTICLE INFO

Article history:
Received 8 June 2015
Received in revised form
7 October 2015
Accepted 8 October 2015
Available online 31 October 2015

Keywords:
Dimethyl ether
Hydrogen
Modelling
Steam reforming
Fluidized bed

ABSTRACT

This study presents a computational fluid dynamic (CFD) study of Dimethyl Ether steam reforming (DME-SR) in a large scale Circulating Fluidized Bed (CFB) reactor. The CFD model is based on Eulerian–Eulerian dispersed flow and solved using commercial software (ANSYS FLUENT). The DME-SR reactions scheme and kinetics in the presence of a bifunctional catalyst of $CuO/ZnO/Al_2O_3$+ZSM-5 were incorporated in the model using in-house developed user-defined function. The model was validated by comparing the predictions with experimental data from the literature. The results revealed for the first time detailed CFB reactor hydrodynamics, gas residence time, temperature distribution and product gas composition at a selected operating condition of 300 °C and steam to DME mass ratio of 3 (molar ratio of 7.62). The spatial variation in the gas species concentrations suggests the existence of three distinct reaction zones but limited temperature variations. The DME conversion and hydrogen yield were found to be 87% and 59% respectively, resulting in a product gas consisting of 72 mol% hydrogen. In part II of this study, the model presented here will be used to optimize the reactor design and study the effect of operating conditions on the reactor performance and products.

Introduction

Hydrogen is currently receiving increasing interest as an alternative source of clean energy and has high potential applications, including the transportation sector and stationary power generation. Traditionally, hydrogen is produced from fossil fuels by steam reforming of natural gas or heavy hydrocarbons; however recently, there is growing research and development activities on hydrogen produced from other sources, such as biomass, methanol (MeOH) and Dimethyl Ether (DME). DME is particularly attractive for hydrogen production because it contains higher mass fraction of hydrogen (13 wt%) and the reforming process can be carried out at a lower temperature (200–350 °C) compared to other options,

* *Corresponding author*. Tel.: +971 6 515 2167; fax: +971 6 515 2979.
E-mail address: ymakkawi@aus.edu (Y.T. Makkawi).

http://dx.doi.org/10.1016/j.ijhydene.2015.10.050

such as natural gas reforming for instance [1,2], hence, less energy intensive.

There is appreciable number of published research papers on methane and methanol steam reforming processes, however there is less focus on DME Steam Reforming (DME-SR), particularly in fluidized bed reactors. As far as the author's knowledge, there are no publications on experimental or computational modelling of the DME-SR in a circulating fluidized bed (CFB) system. Owing to their superior heat transfer, intensive solid–gas mixing and the potential integration with catalyst regeneration within a closed loop dual fluidized bed (DFB), it could be easily argued that the circulating fluidized bed is one of the most important technologies for industrial scale hydrogen production.

Numerical investigations have shown the potential of the DFB in carrying out simultaneous reforming reaction, catalyst regeneration and carbon dioxide capture [3–5]. This has been demonstrated for hydrogen production by methane steam reforming were the reforming reactions and carbon dioxide capture are assumed to take place in one reactor while the sorbent regeneration takes place in a second joint reactor, thus forming a continuous closed loop flow. The DFB system has also been frequently reported as a promising technology for other large scale processes involving solid–gas flow [6,7]. Experimental studies on hydrogen production via catalytic steam reforming of methanol have shown that a fluidized bed reactor has a 20% higher conversion efficiency compared to fixed bed reactors [8]. This is mainly due to the advantages of having larger surface contact area, uniform temperature distribution and better control of the gas residence time.

The DME-SR reaction occurs in two-steps: DME hydrolysis and steam reforming of methanol, with the latter being produced from the first step [9–11]. It is this two-steps reaction that necessities the use of a bifunctional catalyst to facilitate both reactions. However, depending on the catalyst used and the reaction parameters, some side reactions may occur which include water-gas shift reaction (WGSR) and DME decomposition reaction [12]. The catalysts that have been frequently reported in DME-SR are alumina or zeolite acid catalyst in combination with metallic copper oxides [10,13–15]. The zeolite component is the preferred choice as acid site for the hydrolysis of the DME because it promotes reaction at a lower temperature compared to the alumina [16]. It is understood that the alumina catalyst promotes the reverse WGSR while the zeolites acid site promotes the forward reaction. Hence, the zeolite help in increasing the hydrogen yield by converting the carbon monoxide formed during the process to hydrogen and carbon dioxide [17]. The metal based catalyst $CuO/ZnO/Al_2O_3$ has been used in methanol steam reforming studies [18–20]. The same metal catalyst, but with an added ZSM-5 zeolite catalyst, has been recently reported in experimental studies of DME-SR [21]. Such a bifunctional catalyst is suitable for achieving very high hydrogen yield with minimum carbon monoxide produced due to presence of WGSR.

Review of the available literature show that numerical studies on DME-SR in fluidized bed reactors are limited. Feng et al. [22] developed a one-dimensional isotherm plug flow model to simulate DME-SR in a fixed bed reactor with bifunctional catalyst $CuO/ZnO/Al_2O_3$+ZSM-5. The DME hydrolysis reaction was implemented in the model using a simple multi-response objective function with the kinetics derived from the elementary reaction steps of methanol dehydration to DME. Yan et al. [21] conducted a numerical study on DME-SR in a micro-reactor with the same bifunctional catalyst and predicted up to 70–90% DME conversion when operating the reactor within the temperature range of 240–280 °C. Other catalysts, such as mechanically mixed HPA/Al_2O_3 acidic catalyst and Cu/SiO_2 metallic catalyst, have been tested experimentally in a fixed bed reactor and reported to achieve near 100% DME conversion at 290 °C [23]. A Numerical study using STAR-CD software has been reported to investigate the fluid flow, heat transfer and chemical reactions during DME-SR in a fixed bed [12]. The DME-SR kinetics was based on $CuO–NiO/Al_2O_3/ZrO_2$+ZSM-5 catalyst. The results have shown fast decrease of the temperature at the entrance region of the reactor because of the endothermic nature of the DME-SR reaction. Beyond the entrance region, the temperature was found to increase along the axial length of the bed to the exit. Recently, a mathematical model coupling mass, energy and momentum equations has been reported to investigate the DME SR in a novel fluidized bed reactor using Comsol commercial software [24]. The reactor was assumed to be thermally driven by exhaust gas recycling. The result provided useful data on the effect of varying the exhaust gas velocity and other operating parameters on the DME conversion and hydrogen yield.

In this study, which is the first in a series of two, Eulerian–Eulerian model is used to simulate the DME-SR in a CFB reactor, as part of a proposed concept of closed loop DFB system. The model was solved using commercial software (ANSYS FLUENT). The chemical reactions and kinetic in the presence of bifunctional catalyst $CuO/ZnO/Al_2O_3$+ZSM-5 were implemented in the model using in-house developed user-defined function (UDF). The model was first validated by comparison with experimental data [17], then used to show the detailed hydrodynamics and thermochemical behaviour of the CFB reactor at a selected operating conditions. In part II of this study, this model will be used for optimizing the reactor design and studying the effect of operating conditions on the reactor performance and products.

Proposed concept and computational domain

It is proposed that the overall DME-SR process is carried out in an industrial scale DFB system. This system mainly consist of two coupled reactors; one for catalytic steam reforming of the DME and the other the thermal regeneration of the catalyst. The solid and gas mixture leaving both reactors are separated using two cyclones as part of a closed loop system. The arrangement of the reactors and the particulate flow throughout the system is described schematically in Fig. 1. In this study, focus is only made on the DME-SR reactor; hence the cyclones and regeneration reactor are outside the scope of the study. The steam reforming reactor is assumed to operate in a riser mode and has the dimensions of 3 m diameter and 15 m height. The choice of this size is made to replicate commercially proven scale of a CFB reactor (e.g. PYROFLOW CFB system of Goodrich Co in Illinois U.S.A as reported in Ref.

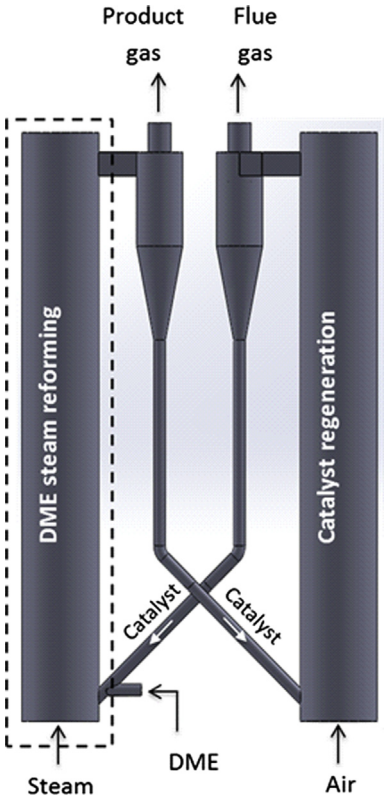

Fig. 1 – Conceptual drawing of the proposed DME-SR process in a dual fluidized bed system. The dotted line indicates the boundary of the computational domain considered in this study.

[7]). The riser is equipped with three openings; at the bottom for introducing the fluidizing steam, at the lower part of the wall for catalyst and DME feeding and at the top part of the wall for exiting the spent catalyst and product gas.

Model formulations

This section presents the main equations for the prediction of the flow hydrodynamics, heat transfer, and reactions taking place during the DME-SR process. The model is in three-dimensional coordinates and takes into consideration the flow of two solid phases (binary mixture), representing a bi-functional catalyst, in addition to the flow of multiple gas species.

Mass conservation, momentum and kinetic energy equations

The multiphase flow mixture in the CFB riser has been simulated using ANSYS FLUENT CFD commercial code (Ver. 14.5) based on Eulerian–Eulerian model with closure equations from the kinetic theory of granular flow (KTGF). In this model, the gas and solid phases (binary solid mixture) are treated as interpenetrating continuum through the volume fractions and the interphase exchange (drag) coefficient. The continuity, momentum and granular energy equations are given as follows:

Conservation of mass:

$$\frac{\partial}{\partial t}(\alpha_i \rho_i) + \nabla\cdot(\alpha_i \rho_i \upsilon_i) = S_i \tag{1}$$

where S is the source term for the volumetric mass transfer rate, α is the volume fraction, υ is the velocity and ρ is the density. The subscript i stands for either the solids (catalyst) or gas phases. Note that S is taken as zero for the solid catalyst due the assumption that no birth or consumption of solids is taking place during the process.

$$\sum_{j=1}^{2} \alpha_{s_j} + \alpha_g = 1 \tag{2}$$

where the subscript $j = 1$ or 2 stands for the two solid phases (catalysts).

Gas phase momentum:

$$\frac{\partial}{\partial t}\left(\alpha_g \rho_g \upsilon_g\right) + \nabla\cdot\left(\alpha_g \rho_g \upsilon_g\right) = -\alpha_g \nabla P_g + \nabla\cdot\bar{\bar{\tau}}_g + \alpha_g \rho_g g - \sum_{j=1}^{2} \beta_{s_j}\left(\upsilon_g - \upsilon_{s_j}\right) \tag{3}$$

where β is the momentum exchange (drag) coefficient between the gas and solid, P is the pressure and $\bar{\bar{\tau}}$ is the gas phase stress tensor and g is the gravity constant.

Solid phase momentum:

$$\frac{\partial}{\partial t}\left(\alpha_{s_i} \rho_{s_i} \upsilon_{s_i}\right) + \nabla\cdot\left(\alpha_{s_i} \rho_{s_i} \upsilon_{s_i}\right) = -\alpha_{s_i}\nabla P_{s_i} + \nabla\cdot\bar{\bar{\tau}}_{s_i} + \alpha_{s_i}\rho_{s_i} g + \beta_{s_i}\left(\upsilon_g - \upsilon_{s_i}\right) + \sum_{j=1}^{2} K_{s_{i,j}}\left(\upsilon_{s_i} - \upsilon_{s_j}\right) \tag{4}$$

where K_{s_i} is the solid–solid momentum exchange coefficient and the subscript $j \neq i$.

Granular kinetic energy:

$$\frac{3}{2}\left[\frac{\partial}{\partial t}\left(\rho_{s_i}\alpha_{s_i}\theta_{s_i}\right) + \nabla\cdot\left(\rho_{s_i}\alpha_{s_i}\theta_{s_i}\upsilon_{s_i}\right)\right] = \left(-P_{s_i}\bar{\bar{I}} + \bar{\bar{\tau}}_{s_i}\right):\nabla\upsilon_{s_i} + \nabla\cdot\left(k_{s_i}\theta_{s_i}\nabla\theta_{s_i}\right) - \gamma\theta_{s_i} + \varphi_{gs_i} \tag{5}$$

where θ is the granular temperature. The terms in the right side represent the generation of energy by the solid stress tensor, the diffusion of energy, the collisional dissipation of energy and the energy exchange between the gas and solid phase respectively.

The conservation equations of species transport in the gas phase are given by:

$$\frac{\partial\left(\alpha_g \rho_g Y_{i,g}\right)}{\partial t} + \nabla\left(\alpha_g \rho_g \upsilon_g Y_{i,g}\right) = -\nabla\cdot\alpha_g \vec{J}_{i,g} + S_i \tag{6}$$

$$\vec{J}_{i,g} = -\left(\rho_g D_{i,g} + \frac{\mu_t}{Sc_t}\right)\nabla Y_{i,g} - D_{T,i,g}\frac{\nabla T}{T} \tag{7}$$

where $Y_{i,g} = 1,2,\ldots n_g$ is the mass fraction of species i in the gas phase, $\vec{J}_{i,g}$ is the diffusion flux, $D_{i,g}$ is the mass diffusion coefficient, and $D_{T,i,g}$ is the thermal diffusion coefficient.

Because of the high fluidizing velocity required to circulate the solid phases, an equation that takes into consideration the flow turbulence is implemented using the widely reported k-epsilon (k-ε) dispersed turbulence model. For details of this the

Table 1 – Constitutive equations for the gas–solid flow hydrodynamics.

Gas-solid interphase exchange (drag) coefficient [25]

$$\beta_{sg} = \frac{3\alpha_s\alpha_g\rho_l}{4v_{r,s}^2 d_s} C_D\left(\frac{Re_s}{v_{r,s}}\right)\left|\vec{v}_s - \vec{v}_g\right|$$

where

$$C_D = \left(0.63 + \frac{4.8}{\sqrt{Re_s/v_{r,s}}}\right)^2$$

$$v_{r,s} = 0.5\left(\alpha_g^{4.14} - 0.06Re_s + \sqrt{(0.062Re_s)^2 + 0.12Re_s(2B - \alpha_g^{4.14}) + \alpha_g^{8.28}}\right)$$

$$B = \begin{cases} 0.8\alpha_g^{1.28}, & \text{if } \alpha_g \le 0.85 \\ \alpha_g^{2.65}, & \text{if } \alpha_g > 0.85 \end{cases}$$

Radial distribution function [26]

$$g_{0s_i} = \left[1 - \left(\frac{\alpha_{s_i}}{\alpha_{s_i,max}}\right)^{1/3}\right]^{-1} + \frac{1}{2}d_{s_i}\sum_{j=1}^{2}\frac{\alpha_{s_j}}{d_{s_j}}$$

where $\alpha_{s,max}$ is the packing limit and its equation for binary mixture can be found in Ref. [26].

Solid–solid drag coefficient [28]

$$K_{s_is_j} = \frac{3\frac{\pi}{2}(1+e_{s_is_j})\alpha_{s_i}\rho_s\alpha_{s_j}\rho_s(d_{s_i}+d_{s_j})^2 g_{0,s_is_j}}{2\pi\rho_s(d_{s_i}^3+d_{s_j}^3)}\left|\vec{u}_{s_i} - \vec{u}_{s_j}\right|$$

Where

$$g_{0,s_is_j} = \frac{d_{s_j}g_{0,s_is_i} + d_{s_i}g_{0,s_js_j}}{d_{s_i}+d_{s_j}}$$

Solid shear stresses [29]

$$\bar{\bar{\tau}}_s = 2S(\mu_{s_i,col} + \mu_{s_i,kin})$$

where

$$\bar{\bar{S}}_s = \frac{1}{2}(\nabla\vec{u}_s + (\nabla\vec{u}_s)^T)$$

$$\mu_{s_i,col} = \left(\frac{4}{5}\alpha_{s_i}\rho_s d_s g_{0s_i}(1+e_{s_i})\sqrt{\frac{\theta_{s_i}}{\pi}}\right)$$

$$\mu_{s_i,kin} = \left(\frac{\alpha_{s_i}\rho_s d_s\sqrt{\pi\theta_{s_i}}}{6(3-e)g_{0s_i}\varepsilon_{s_i}}\left[1 + \frac{2}{5}(1+e_{s_i})(3e_{s_i}-1)g_{0s_i}\alpha_{s_i}\right]\right)$$

Solid phase pressure [26]

$$P_{s_i} = \alpha_{s_i}\rho_{s_i}\theta_{s_i} + \sum_{j=1,j\neq i}^{3}\frac{(d_{s_i}+d_{s_j})^3}{4d_{s_i}^3}g_{0,s_is_j}\rho_{s_i}\alpha_{s_i}\alpha_{s_j}\theta_{s_i}(1+e_{s_is_j})$$

Gas stress tensor [30]

$$\bar{\bar{\tau}}_g = \alpha_g\mu_g(\nabla v_g + \nabla v_g^T) + \alpha_g\left(\lambda_g - \frac{2}{3}\mu_g\right)\nabla\cdot v_g\bar{\bar{I}}$$

Energy dissipation [26]

$$\gamma_{s_i} = 3(1-e^2)\alpha_{s_i}^2\rho_{s_i}g_{0s_i}\theta_{s_i}\left(\frac{4}{d_{s_i}}\sqrt{\frac{\theta_{s_i}}{\pi}}\right)$$

Diffusion coefficient of granular energy [29]

$$\kappa_{\theta_{s_i}} = \frac{150\rho_s d_{s_i}(\pi\theta_{s_i})^{\frac{1}{2}}}{384(e_{s_is_i}+1)g_{0,s_is_i}}\left[1 + \frac{6}{5}\alpha_{s_i}g_{0,s_is_i}(e_{s_is_i}+1)\right]^2 + 2\alpha_{s_i}^2\rho_s d_{s_i}g_{0,s_is_i}(e_{s_is_i}+1)\left(\frac{\theta_{s_i}}{\pi}\right)^{\frac{1}{2}}$$

reader is referred to the reported literature [25–27]. The equations for the gas–solid and solid–solid drag coefficients and the various constitutive equations derived from the KTGF are summarized in Table 1.

Heat transfer equations

The heat balance in the reactor was solved for the solid and gas phases by using the following energy conservation equation for both phases:

$$\frac{\partial}{\partial t}(\alpha_i\rho_i h_i) + \nabla\cdot(\alpha_i\rho_i v_i h_i) = \alpha_i\frac{\partial P_i}{\partial t} + \bar{\bar{\tau}}_i : \nabla v_i - \nabla\cdot q_i + S_i + \sum_{j=1}^{2}Q_{s_jg} \tag{8}$$

where q, S and Q refer to the heat flux, source term for the enthalpy change due to chemical reaction and the volumetric rate of energy transfer, respectively. The subscript i refers to solid or gas and $j = 1$ or 2 refers to the two solid phases (catalysts). Note that, in this analysis the solid–solid heat transfer is ignored because the reactor is operating at a dilute condition. The volumetric rate of energy transfer between the gas and solid phases is given by:

$$Q_{s_jg} = h_{s_jg}A_{s_j}\left(T_{s_j} - T_g\right) \tag{9}$$

where A_s is the interfacial transfer area, T_s and T_g are the solid phases and gas temperatures respectively, and h_{sg} is the volumetric heat transfer coefficient given in terms of the Nusselt number as follows:

$$h_{s_jg} = \frac{k_{s_j}Nu_S}{d_{s_j}} \tag{10}$$

where k_s is the thermal conductivity of the solid phase and Nu_S is the Nusselt number given by Gunn [31] correlation as follow:

$$Nu_{S_j} = \left(7 - 10\alpha_{s_j} + 5\alpha_{s_j}^2\right)\left(1 + 0.7Re_{s_j}^{0.2}Pr^{1/3}\right) + \left(1.33 - 2.4\alpha_{s_j} + 1.2\alpha_{s_j}^2\right)Re_{s_j}^{0.7}Pr^{1/3} \quad (11)$$

DME-SR reactions and kinetics model

The widely reported reaction scheme for catalytic DME-SR involves two major reactions, as noted earlier. This includes a hydrolysis reaction converting the DME to methanol and a steam reforming reaction converting the methanol to hydrogen and carbon dioxide. The proposed reactions and kinetics, as well as the additional side reactions, as described here have all been extracted from various literature sources. Studies [21,22] have shown that within the temperature range of 200–300 °C the DME undergoes catalytic steam reforming (hydrolysis) in the presence of the acid based catalyst ZSM-5 to produce methanol according to the following reaction:

$$CH_3OCH_3 + H_2O \leftrightarrow 2CH_3OH \qquad \Delta H_r^\circ = +24.5\ \text{kJ/mol} \quad (12)$$

The methanol then undergoes steam reforming to generate carbon dioxide and hydrogen enhanced by the presence of the metal based catalysts $CuO/ZnO/Al_2O_3$ according to the following reaction:

$$CH_3OH + H_2O \rightarrow CO_2 + 3H_2 \qquad \Delta H_r^\circ = +49.1\ \text{kJ/mol} \quad (13)$$

Some studies suggested that without the $CuO/ZnO/Al_2O_3$ catalyst the DME reforming process produces methanol only, whereas with the catalyst, hydrogen and carbon dioxide are the major products along with some portion of unreacted methanol and carbon monoxide [12,22].

The widely reported side reactions are associated with the methanol decomposition and the WGSR [18] and these reactions are as follows:

$$CH_3OH \rightarrow CO + 2H_2 \qquad \Delta H_r^\circ = +90\ \text{kJ/mol} \quad (14)$$

$$CO + H_2O \leftrightarrow CO_2 + H_2 \qquad \Delta H_r^\circ = -41.17\ \text{kJ/mol} \quad (15)$$

Li et al. [12] suggested that the WGSR is the only side reaction that may occur in the overeall process. It is also understood that the carbon monoxide production is favoured at higher temperature as the WGSR shifts to the left, which means reduction of hydrogen produced. The complete DME steam reforming reaction scheme used in this study, including the details of the rate equations and kinetics, are given in Table 2.

Model boundary conditions and solution procedure

Model Boundary conditions

In the solution of the model equations, no-slip wall condition was assumed for the gas phase and a slip velocity and granular temperature was specified for the solid phases. The interaction of the solids with the wall was considered by using Johnson and Jackson [34] boundary condition given by the following equations:

$$u_{s_i,w} = -\frac{6\mu_{s_i}\alpha_{s_i,max}}{\sqrt{3\theta_{s_i}}\pi\varphi\rho_s\alpha_{s_i}g_{0,s_i}}\frac{\delta v_{s_i w}}{\delta n} \quad (16)$$

$$\theta_{s_i} = -\frac{k_{s_i}\theta_{s_i}}{\gamma_w}\frac{\delta\theta_{s_i w}}{\delta n} + \frac{\sqrt{3}\pi\varphi\rho_s\alpha_{s_i}v_{s_i w}^2 g_{0s_i}\theta_{s_i}^{\frac{3}{2}}}{6\alpha_{s,max}\gamma_w} \quad (17)$$

where e_{s_i} is the particle-wall restitution coefficient and φ is the specularity coefficient, which is the fraction of collision of particles that transfers significant amount of particle lateral

Table 2 – The various reaction steps and their kinetics used in the DME-SR model.

Steps	Reactions	Rate equations	Reference
DME hydrolysis	$CH_3OCH_3 + H_2O \leftrightarrow 2CH_3OH$	$r_{DME} = r_{DMO^+} = k'_{F,DMO^+}C_{R_i^+}P_{MeOH} - k'_{C,DMO^+}C_{DMO^-}$ (Further details of this reaction and the definition of the symbols can be found in the given references)	[21,22]
MeOH-SR	$CH_3OH + H_2O \rightarrow CO_2 + 3H_2$	$r_R = (1-\varepsilon)\rho_s k_R C_{CH_3OH}$ Where $k_R = C_R[A_1 + B_1 \ln\varnothing]\exp\left(-E_R/RT\right)$ $C_R = 5.5$ is the reforming rate constant, $\varnothing$ is the steam to methanol ratio, A_1 and B_1 are constants (=1.15×10^6 and 9.41×10^5 $m^3\,s^{-1}\,kg^{-1}$ respectively)and $E_R = -84{,}100$ J mol^{-1} is the activation energy	[18,19]
MeOH decomposition	$CH_3OH \rightarrow CO + 2H_2$	$r_D = (1-\varepsilon)\rho_s k_D$ Where $k_D = C_D A_2 \exp\left(-E_D/RT\right)$ $C_D = 5.5$ is the decomposition rate constant, $A_2 = 7.09\times10^7$ mol $s^{-1}\,kg^{-1}$ is a constants and $E_D = -111{,}200$ J mol^{-1} is the activation energy	[18,19,32]
Water gas shift	$CO + H_2O \leftrightarrow CO_2 + H_2$	$r_{WGS} = C_{WGS}k_{WGS}(p_{CO}p_{H_2O} - p_{CO}p_{H_2}/K_{eq})$ Where $K_{eq} = \exp(4577.8/T - 4.33)$ $k_{WGS} = 1.74\times10^{17}(1 - 0.1540\delta + 0.008\delta^2)T^{-8.5}\exp\left(\frac{-35000}{RT}\right)$ $C_{WGS} = 11.2$ is a constant and δ is steam to CO molar ratio	[32,33]

momentum to the wall. The outlet of the reactor was set to "pressure outlet", which ensures the conservation of mass in an open boundary. The boundary at the fluidizing gas and solid catalyst inlets, located at the bottom and side wall of the reactor respectively have been specified as mass flow. In specifying the thermal boundary conditions, the reactor wall was assumed to be perfectly insulated, i.e. no heat flux. The steam, DME and solid catalyst were all introduced to the reactor at a fixed temperature of 300 °C.

Meshing scheme and solution procedure

The geometry of the CFB riser was designed using SOLIDWORKS, a computer-aided design (CAD) software compatible with ANSYS FLUENT code. This was imported into FLUENT simulation platform for meshing. A high quality mesh was obtained by using tetrahedral (patch conforming) meshing method, which allows dividing the domain geometry into tetrahedral shaped cells with refined edges and faces. The mesh quality was checked using skewness and aspect ratio. The skewness value gives indication of the deviation from the ideal tetrahedral cell size while the aspect ratio gives the ratio of longest side of the element to the shortest side. The maximum skewness and aspect ratio were 0.80 and 10.05 respectively, which according to ANSYS FLUENT documentations are within the recommended range for meshing a reactor of the size considered here. In making decision on the number of grids or cells required to accurately predict the behaviour in the simulation domain shown in Fig 2, a detailed grid sensitivity analysis was conducted. Three different cell numbers of 117,000, 211,303 and 400,000 were tested. The predictions have shown minor hydrodynamic differences but a considerabl increase in the computational time at higher cell numbers. Accordingly, 117,000 cells number was used in the simulation. Similarly, the computational time step was set at 0.001 based on careful sensitivity analysis.

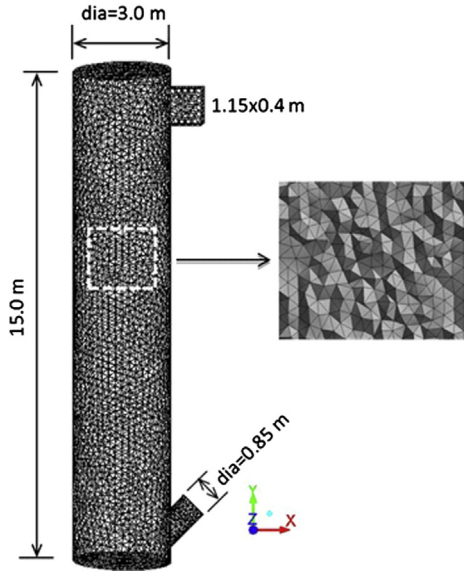

Fig. 2 – The computational domain and meshing of the CFB riser geometry.

Table 3 – The parameters used in the model solution.

Parameters	Values
Specularity coefficient, φ (–)	0.5
Wall-particle restitution coefficient, $e_{s,w}$ (–)	0.8
Particle–particle restitution coefficient, e_s (–)	0.9
Solution time step (s)	0.001
Maximum number of iterations (–)	20
Solution convergence criterion (–)	10^{-3}

Table 4 – The reactor operating conditions used in the simulation.

Parameters	Operating condition
Steam:	
Inlet temperature	300 °C
Flow rate	9.0 (kg/s)
DME:	
Inlet temperature	300 °C
Flow rate	3.0 (kg/s)
Catalyst[a]:	
Particle diameter	150 μm (both catalyst)
Density	1300 kg/m^3 ($CuO/ZnO/Al_2O_3$) 720 kg/m^3 (ZSM-5)
Total mass flow rate	600 kg/s (300 kg/s each catalyst)
Calculated space velocity	37,104 ml g_{cat}^{-1} h^{-1}
Reactor dimensions:	
Diameter	3.0 m
Height	15.0 m

[a] Specified as two separate solid materials: $CuO/ZnO/Al_2O_3$ and ZSM-5.

The gas density was calculated based on the ideal gas law and all the other physical properties of the gas species were selected from FLUENT software library. The gas mixture properties were obtained using mass weighted mixing law. The model was solved using HP Z620 Workstation of 16 core processors (CPU of 2.70 GHz and 32 GB RAM). Because the simulation was carried out in three-dimensional coordinates and in a large scale reactor, the computational time was relatively long compared to similar simulation of a lab scale reactor, mainly due to the large number of cells with the added complexity of chemical reactions. The total computational time required to reach steady state solution was 216 h, corresponding to 50 s real time operation. Summary of the model parameters and the reactor operating conditions considered in the simulation are given in Tables 3 and 4 respectively.

Implementation of the DME-SR reactions

The reactions considered for the DME-SR process, given in Section DME-SR reactions and kinetics model, have been implemented in the main computational model using an *in-house* developed UDF. It is assumed that the two main reactions of DME hydrolysis and methanol steam reforming are initiated and accelerated by the bifunctional catalyst $CuO/ZnO/Al_2O_3$+ZSM-5 with the ZSM-5 group acting as the acid site for enhancing the hydrolysis step of the reaction. The catalyst was introduced to the model as two separate solid phases with the same size and mass flow rate but different densities.

This procedure allowed enabling the UDF to impose the effects of the acidic and metallic functions separately on the different reaction. All the reactions have been implemented as heterogeneous reactions in order to take into consideration the presence of the catalysts and its spatial variations in concentration.

Validation procedure

In order to validate the model, comparison has been made with the experimental data reported by Ref. [17] for DME-SR in a bubbling fluidized bed of 0.022 m diameter with the bed material consisting of the same bifunctional catalyst considered in this study ($CuO/ZnO/Al_2O_3$+ZSM-5). To ensure good grounds of comparision, the exact reactor geometry and operating condition used in the experiment have been applied in the simulation. The meshing method and the solution procedure described above for the CFB riser have also been applied here.

The validation has been made by comparing the prediction with the experimental measurements of the product gas composition, DME conversion (C_{DME}), MeOH conversion (C_{MeOH}), hydrogen yield (Y_{H_2}) and carbon dioxide selectivity (S_{CO_2}). Following [17,22], the DME conversion was given by:

$$C_{DME} = \frac{n_{DME,in} - n_{DME,out}}{n_{DME,in}} \times 100 \quad (18)$$

where $n_{DME,in}$ and $n_{DME,out}$ are the molar flow rate of the DME at the inlet and outlet of the reactor respectively. Similarly the methanol conversion (C_{MeOH}) was given by:

$$C_{MeOH} = \frac{n_{MeOH,prod} - n_{MeOH,out}}{n_{MeOH,prod}} \times 100 \quad (19)$$

where $n_{MeOH,prod}$ and $n_{MeOH,out}$ are the molar flow of methanol produced from the DME pyrolysis reaction and the unreacted methanol leaving with the product gas respectively. The former is assumed to be equal to the number of moles of DME consumed in the process. The percentage of hydrogen yield was given by:

$$Y_{H_2} = \frac{1}{6}\frac{n_{H_2}}{n_{DME,in}} \times 100\% \quad (20)$$

where the number 6 represent the stoichiometric coefficient of the hydrogen component produced in the reactions. The carbon dioxide selectivity was defined in terms of the molar flow ratio of carbon dioxide produced to the total moles of the carbon present in the product as follows:

$$S_{CO_2} = \frac{n_{CO_2}}{n_{CO} + n_{CO_2}} \quad (21)$$

where n_{CO} and n_{CO_2} are the molar flow rate of carbon monoxide and carbon dioxide at the reactor outlet respectively.

Results and discussion

This section presents first a validation of the proposed model by comparing the predictions with the reported experimental data produced by Ref. [17] in a bubbling fluidized bed. This is then followed by presentation of the predicted data and analysis of the CFB performance in terms of the flow hydrodynamics, gas residence time, temperature distribution and product gas composition for a selected operating condition. In part II of this study, a critical assessment of the reactor performance at various operating conditions will be presented.

Validation of the model

Fig. 3 shows a comparison between the model predictions and the experimental data. In Fig. 3a, there is clear reasonable match between the two sets of data. In Fig. 3b, the predicted mole fraction of the hydrogen and DME are also in reasonable agreement with the experimental data, however the carbon monoxide, carbon dioxide and methanol are all over predicted. It is difficult to give precise reasons for such a discrepancy; however it has to be taken into consideration that the model assumes ideal conditions by neglecting the effects of catalyst deactivation. The experimental work of [17] have indicated possible catalyst deactivation by coke deposition on the metallic catalyst at temperatures above 275 °C.

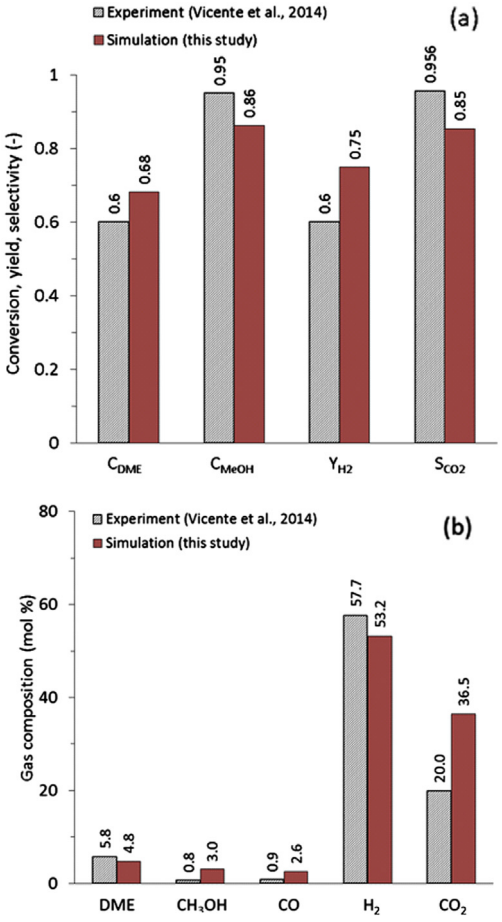

Fig. 3 – Comparison between the predicted and experimental data (a) conversion, yield and selectivity (b) product gas composition (dry basis). Operating conditions: Inlet temperature = 300 °C, space velocity = 0.2 $g_{catalyst}$ h/g_{DME}, P_{DME} = 0.16 bar, steam to DME mass ratio = 1.18 (equivalent to molar ratio of 3).

According to [16,17] such a phenomena could have a complex effect on the equilibrium shift between the DME hydrolysis and methanol steam reforming. Another reason that may have contributed to this discrepancy is the possible formation of small quantity of methane during the process. Some experimental studies have reported presence of small quantities of methane in the product gas believed to be generated from DME decomposition when a strong acidic function or high temperature is used [14,16,17]. In this study, such a reaction is neglected, and so did majority of the reported studies on DME catalytic steam reforming [9,35]. Finally, another factor that is worth noting is the uncertainty about the side reactions that may take place during the DME-SR. A number of researchers have recommended more experimental work to reveal more details about the side reactions and its kinetics.

Hydrodynamic performance in the CFB reactor

Solid/gas distribution and velocities

It is desirable to have homogeneous flow pattern and sufficient gas residence time inside the reactor in order to enhance the DME reforming reactions and increase the hydrogen yield. These can be analysed by looking at the solid volume concentration, which is a measure of the catalyst surface area available for reaction, and by calculating the gas velocity and residence time.

Fig. 4 shows the time-averaged contours of the solid volume fraction and vertical gas/solid velocities in a cross-section at the middle of the reactor. It should be mentioned that, the solid concentration and velocities presented here are for one selected solid phase because both catalysts, CuO/ZnO/Al_2O_3 and ZSM-5, are introduced to the reactor at the same mass flow and their physical properties are very similar. Here, it is clear that the solid concentration is dilute and non-uniform (asymmetric). This non-uniformity is mainly due to the entrance effects (solid feeding from one side of the column). As expected, the solid and gas velocities follow the same flow pattern. The extreme velocity spot near the exit is due to the sharp flow deflection at this region. There is back flow and circulation of the gas and solid phases indicated by the negative or very low velocities in the upper left side and around the solid entrance at the bottom right in the velocities contour plots. Interestingly, these are the regions where the hydrogen concentration is highest, as well be demonstrated later. In part II of this study, the effect of changing the feeding location on the flow hydrodynamics, as well as on the overall thermochemical performance of the reactor, will be discussed in details.

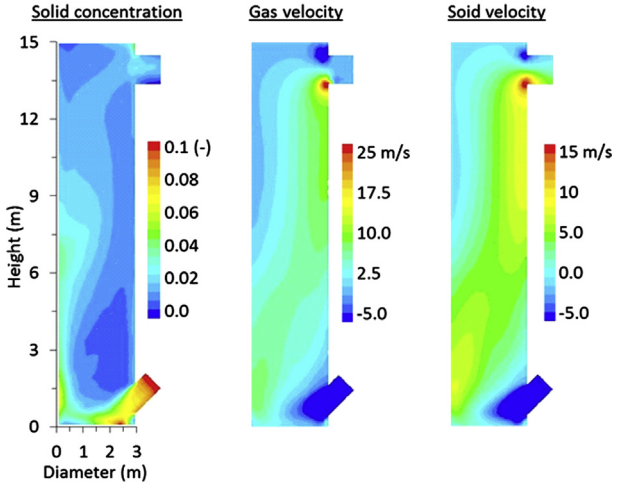

Fig. 4 – Contour plots of the time-averaged solid (catalyst ZSM-5) volume fraction and vertical velocities of the solid and gas phases. The gas and solid velocities have been restricted to 25 m/s and 15 m/s respectively to allow better demonstration of the spatial distribution.

Gas residence time

The gas residence time is an important parameter defining the degree of contact between the gas and solid catalyst within the hot zone of the reactor. The information on the gas velocity, shown earlier in Fig. 4, could be used for a first estimate of the gas residence time. If for simplicity, it is assumed that the flow obeys a plug flow with limited axial velocity variations, then the approximate gas residence time for the case considered here would be 2.8 s. However, since there is clear evidence of considerable gas velocity variations and back mixing in Fig. 4, the gas velocity distribution and a mean gas velocity have to be calculated. For this purpose, an advanced numerical technique based on tracer method has been used. This is carried out by tracking an inert molecule of similar characteristics to the DME and steam mixture injected at the inlet of the reactor at time $t = 0$ in a manner similar to pulse input [36]. The concentration of the tracer exiting the reactor was then monitored as a function of time to give a residence time distribution function $E(t)$ and a mean gas residence time given by the area under the curve $E(t)$, as shown in Fig. 5. The calculated mean gas residence time was 3.92 s. Unfortunately, there is no experimental data on the recommended range of gas residence time for DME-SR in a fluidized bed reactor, however, as a comparison, a study on methanol steam reforming in a micro-channel using copper–zinc catalyst has shown that a residence time of around 1.0 s is sufficient to achieve more than 80% methanol conversion at the temperature of 350 °C [37]. Clearly this is much shorter time than

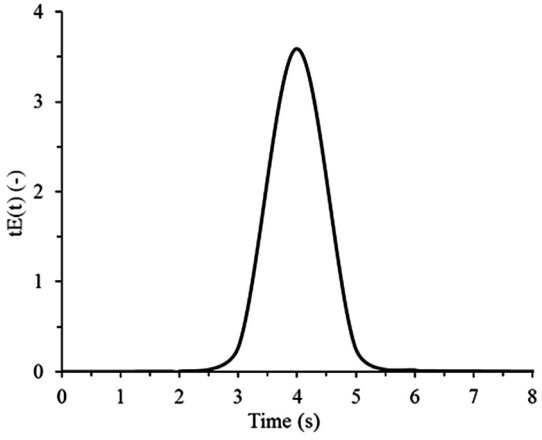

Fig. 5 – The tE(t) curve used for the derivation of mean gas residence time.

what is predicted here because, unlike the methanol reforming, the complete reactions of DME-SR requires additional time to accommodate for the first stage of the DME conversion to produce methanol. It is also recognized that the CFB reactor operates at a dilute suspension condition, thus requires more time for sufficient contact between the catalyst and gas. In part II of this study, further discussion and analysis of the effect of the gas residence time on the DME reforming will be presented.

Thermochemical performance

Spatial distribution of temperature

The majority of the reported studies on DME and methanol steam reforming have been conducted on lab scale fixed bed reactors, with very little reference to the spatial variation of temperature, despite the well documented critical effect of the temperature on the reactor performance. The widely agreed range of temperatures for DME steam reforming using the catalyst considered in this study is within the range of 200–300 °C [21,22]. Though, Takeishi [13] extended this to higher temperatures in the range of 300–350 °C in order to achieve excellent hydrogen production with less CO. The recommended temperature was also reported to be dependent on the weight ratio between Cu and Zn in the CuO/ZnO/Al_2O_3 catalyst. The DME hydrolysis reaction is relatively slow and requires temperature higher than 200 °C, but it has to be noted that the metallic part of the bifunctional catalyst deactivates at temperatures higher than 325 °C as a result of coke deposition [10,17].

Fig. 6 shows the central-line time-averaged axial temperature profile of the gas and the contour plot in a cross-section at the middle of the reactor. In general, Fig. 6a show insignificant overall temperature variation along the reactor height, but there is a noticeable sharp temperature decrease within a limited region between the bottom and above the catalyst entrances level. This is mainly due to the heat being consumed by the DME hydrolysis reaction, which is slightly endothermic. Similar observation has been reported by Li et al. [12] in a fixed bed reactor. The observed temperature non-uniformity seen in the contour plot (Fig. 6b) is a reflection of the asymmetric flow structure and solid back mixing, as noted earlier. At the far top section of the reactor, the temperature slightly increases and this could be attributed to the moderately exothermic WGSR associated with the increase in carbon monoxide formation in this region. This phenomenon is further confirmed by analysing the spatial variation in the product gas composition inside the reactor, as will be discussed in the next section.

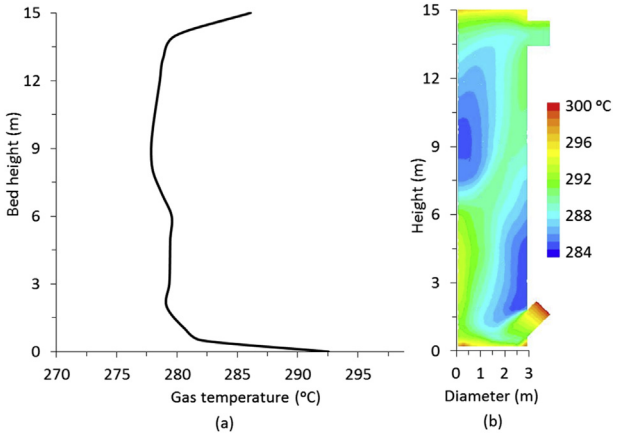

Fig. 6 – Time-averaged gas temperature (a) average axial profile and (b) contour plot.

Spatial distribution of gas species concentration

One of the great advantages in CFD modelling is that it predicts detailed microscopic data that may be difficult to measure experimentally, especially when considering large scale processing unit. Fig. 7 shows the spatial variation in concentration of the gas species inside the reactor after reaching a steady state condition. As expected, both of the reactants (DME and steam) appear with high concentrations at the entrance and then get consumed as they rise towards the top. The hydrogen and the carbon dioxide both appear with high quantities at the top, but with higher concentrations in a limited region near the entrance. The information provided in Fig 7 has been particularly useful in understanding the reactions zones in the CFB reactor as summarized below:

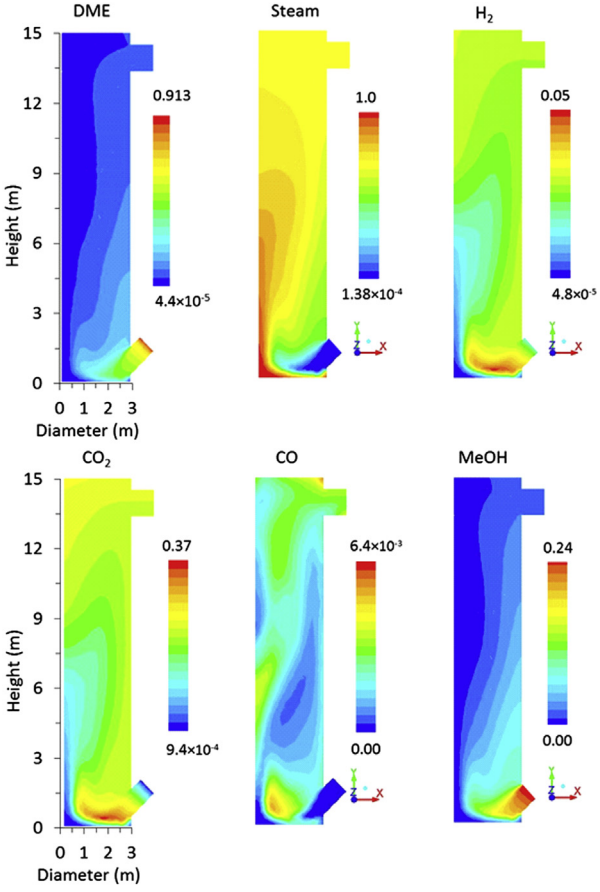

Fig. 7 – The spatial variations of the gas species concentrations in mass fraction.

- The DME is rapidly consumed at a very short entrance length to form methanol. This behaviour matches well the observed sharp drop in temperature in the entrance region due to the endothermic nature of the DME hydrolysis reaction, as noted earlier.
- The methanol, formed from the DME hydrolysis, is rapidly reformed to produce hydrogen and carbon monoxide within the entrance region. This reaction also contributes to the sharp drop of temperature in this region.
- There is evidence of methanol decomposition at the entrance region indicated by the presence of appreciable amount of carbon monoxide in this region.
- The highest hydrogen and carbon dioxide concentrations are found in a small region within the entrance zone, however these are also well spread and with high concentrations at the top of the reactor.
- Because most of the methanol is consumed at the lower part of the reactor, the increased concentration of the carbon monoxide appearing at the top can only be a result of the WGSR. This hypothesis is supported by the sharp increase in temperature at the far top of the reactor as shown earlier in Fig. 6a (WGSR is exothermic).

Based on the above observations, a proposed map of reaction zones in the CFB is shown in Fig. 8. In reality, it is not expected to see clear cut boundaries, and the transition from one zone to another is most probably gradual and overlapping. Further simulations have shown that the reaction zones proposed here remain generally applicable to wider operating conditions, as will be demonstrated in part II of this study.

Product gas composition

Fig. 9 shows the molar compositions of the product gas in dry basis at the outlet of the CFB reactor. The product gas mainly consists of hydrogen and carbon monoxide, representing a total of 95%, with the remaining 5% consisting of unreacted DME and MeOH in addition to carbon monoxide. Using this data, the calculated DME conversion and hydrogen yield were found to be 87% and 59% respectively. This is relatively a high DME conversion and hydrogen yield compared to most of the reported experimental and numerical studies in fixed and bubbling bed reactors operating at 300 °C [e.g. 11,22]. At a lower temperature within the range of 200 °C, the equilibrium DME conversion has been reported to be less than 20% [21,22]. There is an argument that DME hydrolysis reaction is the rate controlling step in the over DME-SR process and that the DME conversion rate can be increased by enhancing the methanol steam reforming [12]. It is therefore plausible to attribute the high DME conversion predicted here to the contribution of temperature and/or the metal part of the bifunctional catalyst ($CuO/ZnO/Al_2O_3$), which both lead to increasing the methanol steam reforming. The carbon dioxide concentration in the product gas is the second highest with the calculated selectivity of 97.3%. This comes at the expense of the carbon monoxide concentration, which is consumed by the forward WGSR. In part II of this study, detailed parametric analysis of the effect of the operating condition on the product gas composition will be presented.

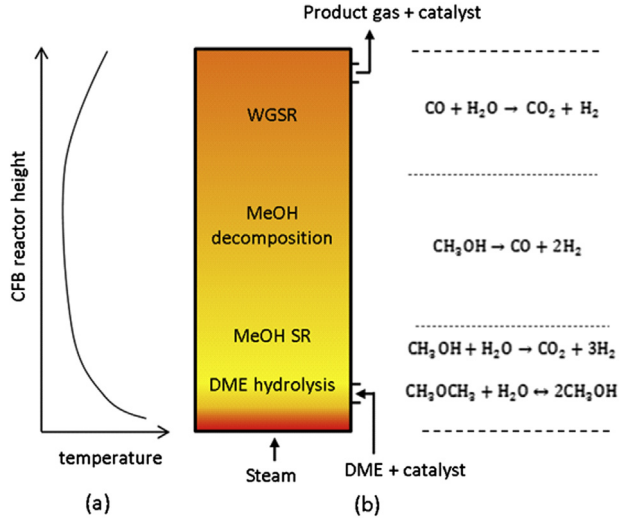

Fig. 8 – Schematic description of the DME-SR reaction zones and the corresponding temperature profile in the CFB reactor.

Conclusions

A computational model capable of predicting the flow hydrodynamics, heat transfer and reactions during DME steam reforming (DME-SR) in a large scale circulating fluidized bed (CFB) reactor has been presented and validated with experimental data from the literature. This is the first reported model of DME-SR in a CFB reactor developed as part of a proposed closed loop dual fluidized bed (DFB) system concept. The model, which is solved using ANSYS FLUENT commercial software, was based on Eulerian–Eulerian approach with the reactions and kinetics adopted from the literature and implemented using a user-defined function (UDF). The model was found to produce satisfactory accurate data within a reasonable computational time despite of the large scale reactor considered.

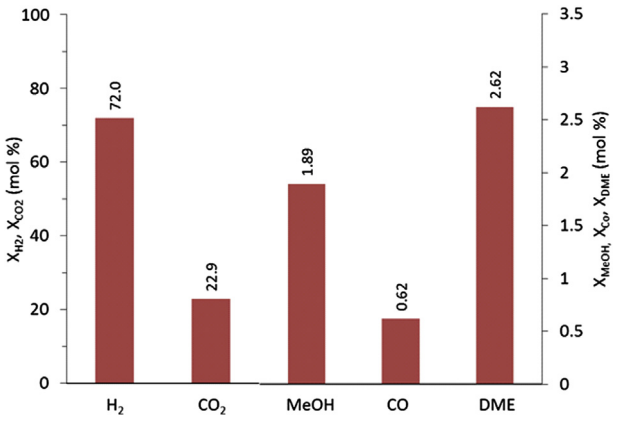

Fig. 9 – The product gas composition at exit of the reactor in mole percentage (on dry basis). Note that the left y-axis represent the hydrogen and carbon monoxide and the right axis represent the MeOH, DME and carbon monoxide.

The hydrodynamics show axisymmetric flow structure, mainly due to the entrance of solid catalysts from one side of the reactor. The DME conversion and the hydrogen yield for the selected case of operating condition of 300 °C and steam to DME mass ratio of 3 (equivalent to 7.62 M ratio) was found to be 87% and 59% respectively. The gas species distributions together with the predicted hydrodynamics suggest that the DME hydrolysis and methanol steam reforming both occur at the bottom of the reactor. These reactions, which are endothermic, result in the reduction of the reactor temperature around the bottom zone. However, the overall temperature variations in the reactor are insignificant. Towards the top part of the reactor, the forward WGSR is predominant. This is associated with a limited increase in temperature around the top. In the middle to the upper part of the reactor, methanol decomposes to produce carbon monoxide and more hydrogen.

With the limited knowledge of DME-SR in industrial scale CFB, the model developed in this study will be particularly useful in further development of the process by providing a robust tool for parametric analysis, reactor design and process optimization, as will be demonstrated in part II of this study.

Acknowledgement

This research has been financially supported by the EPSRC (Ref EP/J501797/1).

Nomenclature

A_1, A_2, B_1	pre-exponential term in the Arrhenius expression, s^{-1}
C_D	decomposition reaction constant (–)
C_μ, $C_{1\varepsilon}$,$C_{2\varepsilon}$	constants (–)
$C_{fr,sisj}$	friction coefficient between solid phases i and j (–)
C_R	methanol steam reforming modification constant (–)
C_{WGS}	water gas shift reaction constant (–)
C_i	concentration of species, mol m^{-3}
$D_{T,i,g}$	thermal diffusion coefficient, kg m^{-2} s^{-1}
d_s	particle diameter of solid phase, m
E_i	activation energy of reaction, J mol^{-1}
e_{sisj}	particle–particle restitution coefficient (–)
$e_{si,w}$	particle-wall restitution coefficient (–)
g_0	radial distribution function (–)
g	gravity, m s^{-2}
$G_{k,g}$	production of turbulent kinetic energy, kg m^{-1} s^{-2}
$\bar{\bar{I}}$	unit vector (–)
$\overrightarrow{J}_{i,g}$	diffusion flux of species i, kg m^{-2} s^{-1}
h_q	specific enthalpy of q phase, J kg^{-1}
k_g	turbulence kinetic energy, m^2 s^{-2}
K_{eq}	water gas shift equilibrium constant, K^{-1}
k_R	methanol steam reforming rate constant, m^3 kg^{-1} s^{-1}
k_{WGS}	water gas shift rate constant, mol m^{-3} s^{-1} K^{-1} pa^{-2}
P	pressure, pa
P_i	partial pressures of gas components, bar
R	gas constant, J mol^{-1} K^{-1}
Re_s	Reynolds number of solid phase (–)
r_D	rate of methanol decomposition, mol m^{-3} s^{-1}
r_R	rate of reaction for methanol steam reforming, mol m^{-3} s^{-1}
r_{DME}	rate of reaction of DME, mol kg-cat^{-1} s^{-1}
T	temperature, °C
$v_{r,s}$	particle terminal velocity, m s^{-1}
v	velocity, m s^{-1}
$Y_{i,g}$	mass fraction of species i in the gas phase (–)

Greek letters

α	volume fraction (–)
β	momentum exchange (drag) coefficient, kg m^{-3} s^{-1}
$\gamma_{\theta_{s_i}}$	collisional energy dissipation, kg m^{-1} s^{-3}
θ_{s_i}	granular temperature of solid phase i, m^2 s^{-2}
$\kappa_{\theta_{s_i}}$	diffusion coefficient of granular energy, kg m^{-1} s^{-1}
$\mu_{l,g}$	viscosity of gas phase due to laminar flow, kg m^{-1} s^{-2}
$\mu_{t,g}$	viscosity of gas phase due to turbulent flow, kg m^{-1} s^{-2}
$\mu_{s_i,col}$	viscosity of solid phase i due to collision, kg m^{-1} s^{-1}
$\mu_{s_i,kin}$	viscosity of solid phase i due to kinetics, kg m^{-1} s^{-1}
ρ	densities respectively, kg m^{-3}
$\bar{\bar{\tau}}$	shear stress tensor, kg m^{-1} s^{-2}
σ_k,σ_ε	constants (–)
$\varnothing$	molar ratio of steam to methanol (–)
φ	Specularity coefficient

REFERENCES

[1] Verykios XE. Catalytic dry reforming of natural gas for the production of chemicals and hydrogen. Int J Hydrogen Energy 2003;28:1045–63. http://dx.doi.org/10.1016/S0360-3199(02)00215-X.

[2] Pamela S, Margaret K. Life cycle assessment of hydrogen production via natural Gas steam reforming. Technical Report (NREL/TP-570–27637). National Renewable Energy Laboratory; 2001.

[3] Wang Y, Chao Z, Jakobsen H. 3D simulation of bubbling fluidized bed reactors for sorption enhanced steam methane reforming processes. J Nat Gas Sci Eng 2010;2:105–13. http://dx.doi.org/10.1016/j.jngse.2010.04.004.

[4] Wang Y, Chao Z, Chen D, Jakobsen H. SE-SMR process performance in CFB reactors: simulation of the CO_2 adsorption/desorption processes with CaO based sorbents. Int J Greenh Gas Control 2011;5:489–97. http://dx.doi.org/10.1016/j.ijggc.2010.09.001.

[5] Wang J, Wang Y, Jakobsen H. The modeling of circulating fluidized bed reactors for SE-SMR process and sorbent regeneration. Chem Eng Sci 2014;108:57–65. http://dx.doi.org/10.1016/j.ces.2013.12.012.

[6] Larsson A, Seemann M, Neves D, Thunman H. Evaluation of performance of industrial-scale dual fluidized bed gasifiers using the chalmers 2-4-MWth gasifier. Energy Fuels 2013;27:6665–80. http://dx.doi.org/10.1021/ef400981j.

[7] Chalermsinsuwan B, Piumsomboon P, Gidaspow D. A computational fluid dynamics design of a carbon dioxide sorption circulating fluidized bed. AIChE J 2010;56:2805–24. http://dx.doi.org/10.1002/aic.12213.

[8] Shi Y, Du X, Yang L, Sun Y, Yang Y. Experiments on hydrogen production from methanol steam reforming in fluidized bed reactor. Int J Hydrogen Energy 2013;38:13974–81. http://dx.doi.org/10.1016/j.ijhydene.2013.08.073.

[9] Yang M, Men Y, Li S, Chen G. Hydrogen production by steam reforming of dimethyl ether over ZnO–Al_2O_3 bi-functional

catalyst. Int J Hydrogen Energy 2012;37:8360–9. http://dx.doi.org/10.1016/j.ijhydene.2012.02.070.
[10] Kawabata T, Matsuoka H, Shishido T, Li D, Tian Y, Sano T. Steam reforming of dimethyl ether over ZSM-5 coupled with $Cu/ZnO/Al_2O_3$ catalyst prepared by homogeneous precipitation. Appl Catal A General 2006;308:82–90. http://dx.doi.org/10.1016/j.apcata.2006.04.032.
[11] Ereña J, Vicente J, Aguayo AT, Olazar M, Bilbao J, Gayubo AG. Kinetic behaviour of catalysts with different $CuO-ZnO-Al_2O_3$ metallic function compositions in DME steam reforming in a fluidized bed. Appl Catal B Environ 2013;142–143:315–22. http://dx.doi.org/10.1016/j.apcatb.2013.05.034.
[12] Li C, Wang Y, Fan P. Numerical analysis and experimental study of hydrogen production from dimethyl ether steam reforming. Sci China Chem 2012;55:1982–7. http://dx.doi.org/10.1007/s11426-012-4603-0.
[13] Takeishi K. Steam reforming of dimethyl ether. Appl Catal A General 2004;260:111–7. http://dx.doi.org/10.1016/j.apcata.2003.10.006.
[14] Faungnawakij K, Tanaka Y, Shimoda N, Fukunaga T, Kikuchi R, Eguchi K. Hydrogen production from dimethyl ether steam reforming over composite catalysts of copper ferrite spinel and alumina. Appl Catal B Environ 2007;74:144–51. http://dx.doi.org/10.1016/j.apcatb.2007.02.010.
[15] Feng D, Zuo Y, Wang D, Wang J. Steam reforming of dimethyl ether over coupled ZSM-5 and Cu-Zn-based catalysts. Chin J Catal 2009;30:223–9. http://dx.doi.org/10.1016/S1872-2067(08)60098-4.
[16] Gayubo AG, Vicente J, Ereña J, Oar-Arteta L, Azkoiti MJ, Olazar M. Causes of deactivation of bifunctional catalysts made up of $CuO-ZnO-Al_2O_3$ and desilicated HZSM-5 zeolite in DME steam reforming. Appl Catal A General 2014;483:76–84. http://dx.doi.org/10.1016/j.apcata.2014.06.031.
[17] Vicente J, Eren J, Oar-arteta L, Olazar M, Bilbao J, Gayubo AG. Effect of operating conditions on dimethyl ether steam reforming in a fluidized bed reactor with a CuO- ZnO- Al_2O_3 and desilicated ZSM-5 zeolite bifunctional catalyst. Industrial Eng Chem Res 2014;53:3462–71.
[18] Suh JS, Lee MT, Greif R, Grigoropoulos CP. A study of steam methanol reforming in a microreactor. J Power Sources 2007;173:458–66. http://dx.doi.org/10.1016/j.jpowsour.2007.04.038.
[19] Amphlett J, Creber KA, Davies J, Mann R, Peppley B, Stokes D. Hydrogen production by steam reforming of methanol for polymer electrolyte fuel cells. Int J Hydrogen Energy 1994;19:131–7.
[20] Nehe P, Kumar S. Methanol reformation for hydrogen production from a single channel with cavities. Int J Hydrogen Energy 2013;38:13216–29. http://dx.doi.org/10.1016/j.ijhydene.2013.07.119.
[21] Yan F, Ye W, Guo Q, Huang L, Li B, Luo M. Numerical simulation and experimental study of hydrogen production from dimethyl ether steam reforming in a micro-reactor. Int J Hydrogen Energy 2014;39:18642–9. http://dx.doi.org/10.1016/j.ijhydene.2014.02.133.
[22] Feng D, Wang Y, Wang D, Wang J. Steam reforming of dimethyl ether over $CuO-ZnO-Al_2O_3-ZrO_2$ + ZSM-5: a kinetic study. Chem Eng J 2009;146:477–85. http://dx.doi.org/10.1016/j.cej.2008.11.005.
[23] Galvita VV, Semin GL, Belyaev VD, Yurieva TM, Sobyanin V. Production of hydrogen from dimethyl ether. Appl Catal a-General 2001;216:85–90. http://dx.doi.org/10.1016/S0926-860X(01)00540-3.
[24] Li C, Gao Y, Wu C. Modeling and simulation of hydrogen production from dimethyl ether steam reforming using exhaust gas. Int J Energy Res 2015;39:1272–9. http://dx.doi.org/10.1002/er.3330.
[25] Syamlal M, O'Brien T. Computer simulation of bubbles in a fluidized bed. AIChE Symp Ser 1989;85:22–31.
[26] Lun CKK, Savage SB, Jeffrey DJ, Chepurniy N. Kinetic theories for granular flow: inelastic particles in couette flow and slightly inelastic particles in a general flowfield. J Fluid Mech 1984;140:223. http://dx.doi.org/10.1017/S0022112084000586.
[27] Fedors RF, Landel RF. An empirical method of estimating the void fraction in mixtures of uniform particles of different size. Powder Technol 1979;23:225–31. http://dx.doi.org/10.1016/0032-5910(79)87011-4.
[28] Syamlal M. Particle-particle drag term in a multiparticle model of fluidization. Springfield, VA: National Technical Information Service; 1987. Topical Report, DOE/MC/21353-2373, NTIS/DE87006500.
[29] Syamlal M, Rogers W, O'Brien TJ. MFIX documentation. In: Theory guide, vol.1. National Technical Information Service; 1993.
[30] ANSYS Fluent Theory Guide Pennsylvania. 2013.
[31] Gunn DJ. Transfer of heat or mass to particles in fixed and fluidised beds. Int J Heat Mass Transf 1978;21:467–76. http://dx.doi.org/10.1016/0017-9310(78)90080-7.
[32] Chein R, Chen YC, Chung JN. Numerical study of methanol-steam reforming and methanol-air catalytic combustion in annulus reactors for hydrogen production. Appl Energy 2013;102:1022–34. http://dx.doi.org/10.1016/j.apenergy.2012.06.010.
[33] Chen W, Lin M, Jiang T, Chen M. Modeling and simulation of hydrogen generation from high-temperature and low-temperature water gas shift reactions. Int J Hydrogen Energy 2008;33:6644–56. http://dx.doi.org/10.1016/j.ijhydene.2008.08.039.
[34] Johnson PC, Jackson R. Friction akollisional constitutive relations for granular materials, with application to plane shearing. J Fluid Mech 1987;176:67–93.
[35] Semelsberger TA, Borup RL, Greene HL. Dimethyl ether (DME) as an alternative fuel. J Power Sources 2006;156:497–511. http://dx.doi.org/10.1016/j.jpowsour.2005.05.082.
[36] Fogler SH. Elements of chemical reaction engineering. 4th ed. New Jersey: Pearson Education, Inc; 2006.
[37] Kuznetsov VV, Vitovsky OV. Hydrogen production by methanol steam reforming in an annular microchannel on a Cu-ZnO catalyst. J Eng Thermophys 2008;17:191–5. http://dx.doi.org/10.1134/S1810232808030041.